Published for SISSA by Springer

Received: *August 14, 2023*
Revised: *January 30, 2024*
Accepted: *March 29, 2024*
Published: *May 17, 2024*

Measurement of branching-fraction ratios and CP asymmetries in $B^{\pm} \to D_{CP\pm}K^{\pm}$ decays at Belle and Belle II

The Belle and Belle II collaboration

E-mail: coll-publications@belle2.org

Abstract: We report results from a study of $B^{\pm} \to DK^{\pm}$ decays followed by D decaying to the CP-even final state $K^{+}K^{-}$ and CP-odd final state $K^0_S\pi^0$, where D is an admixture of D^0 and $\bar{D}^0$ states. These decays are sensitive to the Cabibbo-Kobayashi-Maskawa unitarity-triangle angle ϕ_3. The results are based on a combined analysis of the final data set of $772 \times 10^6 B\bar{B}$ pairs collected by the Belle experiment and a data set of $198 \times 10^6 B\bar{B}$ pairs collected by the Belle II experiment, both in electron-positron collisions at the $\Upsilon(4S)$ resonance. We measure the CP asymmetries to be $\mathcal{A}_{CP+} = (+12.5 \pm 5.8 \pm 1.4)\%$ and $\mathcal{A}_{CP-} = (-16.7 \pm 5.7 \pm 0.6)\%$, and the ratios of branching fractions to be $\mathcal{R}_{CP+} = 1.164 \pm 0.081 \pm 0.036$ and $\mathcal{R}_{CP-} = 1.151 \pm 0.074 \pm 0.019$. The first contribution to the uncertainties is statistical, and the second is systematic. The asymmetries $\mathcal{A}_{CP+}$ and $\mathcal{A}_{CP-}$ have similar magnitudes and opposite signs; their difference corresponds to 3.5 standard deviations. From these values we calculate 68.3% confidence intervals of $(8.5^{\circ} < \phi_3 < 16.5^{\circ})$ or $(84.5^{\circ} < \phi_3 < 95.5^{\circ})$ or $(163.3^{\circ} < \phi_3 < 171.5^{\circ})$ and $0.321 < r_B < 0.465$.

Keywords: B Physics, CKM Angle Gamma, CP Violation, e^{+}-e^{-} Experiments

ArXiv ePrint: 2308.05048

https://doi.org/10.1007/JHEP05(2024)212

JHEP05(2024)212

Contents

1 Introduction

The Cabibbo-Kobayashi-Maskawa (CKM) matrix parameterizes quark mixing in the standard model [1, 2]. The angle ϕ_3, also called γ, is the phase of a product of its elements $-V_{\mathrm{ud}}V^*_{\mathrm{ub}}/V^*_{\mathrm{cd}}V_{\mathrm{cb}}$. Theoretical relationships connecting the angle ϕ_3 with rates and CP asymmetries of the decays $B^{\pm} \to DK^{\pm}$, where D is an admixture of D^0 and $\overline{D}^0$ states, are reliable and can be used for precise direct measurements of ϕ_3. Any inconsistency between direct measurements of ϕ_3 and the value inferred from global CKM fits performed without this information would show that the CKM mechanism is not a complete description of CP violation and reveal effects of physics beyond the standard model. Gronau, London, and Wyler (GLW) proposed a method to extract ϕ_3 using decays in which the neutral D, $D_{CP\pm}$, is reconstructed as a CP eigenstate [3, 4]. We use this method to determine ϕ_3 using combined data sets of the Belle and Belle II experiments.

We measure CP asymmetries,

$$\mathcal{A}_{CP\pm} \equiv \frac{\mathcal{B}(B^- \to D_{CP\pm}K^-) - \mathcal{B}(B^+ \to D_{CP\pm}K^+)}{\mathcal{B}(B^- \to D_{CP\pm}K^-) + \mathcal{B}(B^+ \to D_{CP\pm}K^+)}, \tag{1.1}$$

and the ratio of branching fractions for decays in which the D is reconstructed as a CP eigenstate and decays in which the D is reconstructed in a flavor-specific state:

$$\mathcal{R}_{CP\pm} \equiv \frac{\mathcal{B}(B^- \to D_{CP\pm}K^-) + \mathcal{B}(B^+ \to D_{CP\pm}K^+)}{(\mathcal{B}(B^- \to D_{\mathrm{flav}}K^-) + \mathcal{B}(B^+ \to \overline{D}_{\mathrm{flav}}K^+))/2}. \tag{1.2}$$

JHEP05(2024)212

This ratio can be expressed as

$$\mathcal{R}_{CP\pm} \approx \frac{R_{CP\pm}}{R_{\text{flav}}}, \tag{1.3}$$

where

$$R_{CP\pm} \equiv \frac{\mathcal{B}(B^- \to D_{CP\pm}K^-) + \mathcal{B}(B^+ \to D_{CP\pm}K^+)}{\mathcal{B}(B^- \to D_{CP\pm}\pi^-) + \mathcal{B}(B^+ \to D_{CP\pm}\pi^+)}, \tag{1.4}$$

and

$$R_{\text{flav}} \equiv \frac{\mathcal{B}(B^- \to D_{\text{flav}}K^-) + \mathcal{B}(B^+ \to \overline{D}_{\text{flav}}K^+)}{\mathcal{B}(B^- \to D_{\text{flav}}\pi^-) + \mathcal{B}(B^+ \to \overline{D}_{\text{flav}}\pi^+)}. \tag{1.5}$$

In these ratios of branching fractions, most potential systematic uncertainties, such as those from reconstruction efficiencies and the known D branching fractions, cancel. The approximation in equation (1.3) is an equality if CP is conserved in the $B^\pm \to D\pi^\pm$ decay. Neglecting the small effects of D mixing and CP violation in the D^0 decay [5], we relate $\mathcal{R}_{CP\pm}$ and $\mathcal{A}_{CP\pm}$ to ϕ_3, the ratio r_B of the magnitudes of the suppressed to favored $B^\pm \to DK^\pm$ amplitudes, and the relative CP-conserving phase δ_B between them [6]:

$$\mathcal{R}_{CP\pm} = 1 + r_B^2 \pm 2r_B \cos\delta_B \cos\phi_3, \tag{1.6}$$

$$\mathcal{A}_{CP\pm} = \pm 2r_B \sin\delta_B \sin\phi_3 \,/\, \mathcal{R}_{CP\pm}. \tag{1.7}$$

The current precision on ϕ_3 is about 3.5° [6, 7], dominated by recent measurements from the LHCb experiment [8]. The Belle experiment reported a ϕ_3-related measurement using the ADS method [9, 10] for $B^\pm \to DK^\pm$ decays with $D \to K^\pm\pi^\mp$ using its full data set [11]. A measurement using the BPGGSZ method [12, 13] for $B^\pm \to Dh^\pm$ decays with $D \to K_S^0 h^\pm h^\mp$, where h is a pion or kaon, using the full Belle data set and $128\,\text{fb}^{-1}$ of data from Belle II was reported recently [14]. However, Belle reported results using the GLW $B^\pm \to D^{(*)}K^\pm$ decays based only a fraction of its full data sample [15]. Here we report results for $B^\pm \to D_{CP\pm}K^\pm$ for the CP-even D final state K^+K^- and the CP-odd final state $K_S^0\pi^0$ based on the full Belle data set and also a fraction of the available data from Belle II. These results supersede those of ref. [15].

2 Data samples and detectors

We analyze samples containing 772×10^6 and 198×10^6 $B\overline{B}$ pairs collected in electron-positron collisions at the $\Upsilon(4S)$ resonance with the Belle and Belle II detectors. The integrated luminosities of the corresponding data sets are $711\,\text{fb}^{-1}$ and $189\,\text{fb}^{-1}$ for Belle and Belle II. Belle operated at the KEKB asymmetric-energy collider with electron- and positron-beam energies of 8 GeV and 3.5 GeV [16, 17], respectively. Belle II operates at its successor, SuperKEKB, designed to deliver thirty times higher instantaneous luminosity than KEKB, with electron and positron beam energies of 7 GeV and 4 GeV [18], respectively.

The Belle detector [19, 20] was a large-solid-angle magnetic spectrometer that consisted of a silicon vertex detector, a 50-layer central drift chamber, an array of aerogel threshold Cherenkov counters, a barrel-like arrangement of time-of-flight scintillation counters, and an electromagnetic calorimeter, all located within a superconducting solenoid coil that provided

JHEP05(2024)212

a uniform 1.5 T magnetic field collinear with the beams. An iron flux-return yoke located outside the coil was instrumented to detect K_L^0mesons and muons.

The Belle II detector [21] is an upgrade with several new subdetectors designed to handle the significantly larger beam-related backgrounds of the new collider. It consists of a silicon vertex detector comprising two inner layers of pixel detectors and four outer layers of double-sided silicon strip detectors, a 56-layer central drift chamber, a time-of-propagation detector in the central detector volume and an aerogel ring-imaging Cherenkov detector in the forward region (with respect to the electron-beam's direction) for charged particle identification (PID), and an electromagnetic calorimeter, all located inside the same solenoid as used for Belle. A flux return outside the solenoid is instrumented with resistive-plate chambers, plastic scintillator modules, and an upgraded read-out system to detect muons, K_L^0 mesons, and neutrons.

We use simulated data to optimize selection criteria, determine detection efficiencies, train multivariate discriminants, identify sources of background, and obtain our fit models. The EvtGen software package is used to simulate the $e^+e^- \to \Upsilon(4S) \to B\bar{B}$ process and our signal decays [22]. The KKMC [23] and Pythia [24] generators are used to simulate the $e^+e^- \to q\bar{q}$ continuum, where q indicates a u, d, s or c quark. For Belle, the Geant3 package [25] was used to model the detector response, whereas for Belle II the Geant4 package [26] is used. To account for final-state radiation, the Photos package [27] is used.

3 Reconstruction and candidate selection

We use the Belle II analysis software framework to reconstruct both Belle and Belle II data [28–30]. Owing to the different performance of the detectors, separate sets of selection criteria are used for each data set.

Online data-selection criteria are based on requirements of a minimum number of charged particles and observed energy in an event. They are fully efficient for signal and strongly suppress low-multiplicity events. In the offline analysis, reconstructed charged-particle trajectories (tracks) are required to have distances from the e^+e^- interaction point (IP) smaller than 0.2 cm in the plane transverse to the beams, and smaller than 1.0 cm along the beam direction. Charged kaon and pion candidates are identified based on information from PID detectors and the specific ionisation measured in the drift chamber. We use the ratio $\mathcal{L}(K/\pi) \equiv \mathcal{L}(K)/[\mathcal{L}(K) + \mathcal{L}(\pi)]$ to identify the type of charged particles, where $\mathcal{L}(h)$ is the likelihood for a kaon or pion to produce the signals observed in the detectors. Charged particles with $\mathcal{L}(K/\pi) > 0.6$ are identified as kaons, and those with $\mathcal{L}(K/\pi) < 0.6$ as pions. To mitigate pion misidentification in the Belle II data, we remove tracks with a polar angle $\theta > 120^\circ$, since no PID detector covers this region [31]. No such veto is necessary for Belle data because the larger KEKB boost results in essentially all tracks being within the acceptance of the PID detectors. The kaon-identification efficiency and the rate to misidentify a pion as kaon are quantitatively given in section 4.

We reconstruct K_S^0 candidates in their $\pi^+\pi^-$ final state by forming each from a pair of oppositely charged particles (assuming they are pions) with a common vertex and mass in the range [486, 509] MeV/c^2 for Belle data and [491, 504] MeV/c^2 for Belle II data. These ranges correspond to 3σ in resolution in either direction from the known K^0 mass. To improve the purity of the K_S^0 sample, we reject combinatorial background using neural networks for Belle data and boosted decision trees for Belle II data [14, 32, 33]. Five input variables are common to the Belle and Belle II discriminators: the angle between the K_S^0 momentum and the direction from the IP to the K_S^0 decay vertex; the distance-of-closest-approach to the IP of the pion tracks; the flight distance of the K_S^0 in the plane transverse to the beams; and the difference between the measured and known K_S^0 masses divided by the uncertainty of the measured mass. The Belle discriminator uses seven additional variables, including the K_S^0 momentum and the shortest distance between the two track helices projected along the beam direction [32, 33]. Each K_S^0 momentum is recalculated from a fit of the pion momenta that constrains them to a common origin.

We reconstruct π^0 candidates via their decays to two photons. In Belle data, each photon is required to have an energy above 50 MeV; in Belle II data, each photon is required to have an energy above 80 MeV if detected in the forward endcap, 30 MeV if detected in the barrel, and 60 MeV if in the backward endcap. Each photon candidate must also be unassociated with any track and have an energy-deposition distribution in the calorimeter consistent with an electromagnetic shower. Each π^0 candidate must have a mass in the range $[120, 145]$ MeV/c^2, corresponding to 2.5σ in resolution on either side of the known π^0 mass, and momentum above 0.6 GeV/c. Each π^0 momentum is recalculated from a fit of the photon momenta that constrains them to a common origin and the diphoton mass to the known mass of the π^0.

A D candidate is formed from combinations of K^- and π^+, K^+ and K^-, and K_S^0 and π^0 candidates. The mass of each D candidate is required to be consistent with the known D mass [6] within $[-20, +20]$ MeV/c^2 in Belle data and $[-12, +12]$ MeV/c^2 in Belle II data for $D \to K^\pm h^\mp$ decays; and within $[-64, +47]$ MeV/c^2 in Belle data and $[-53, +36]$ MeV/c^2 in Belle II data for the $D \to K_S^0\pi^0$ decays. These ranges are approximately 3σ in resolution on either side of the known mass. Each D momentum is recalculated from a fit of the momenta of its decay products that constrains them to a common origin and their invariant mass to the known mass of the D meson.

A B candidate is formed from a D candidate and an $h^\pm$ candidate. To select signal candidates, we use the beam-energy-constrained mass,

$$M_{\mathrm{bc}} \equiv c^{-2}\sqrt{E_{\mathrm{beam}}^{*2} - |\vec{p}_B c|^2}, \tag{3.1}$$

and the energy difference, $\Delta E \equiv E_B - E^*_{\mathrm{beam}}$, calculated from the B energy E_B, momentum $\vec{p}_B$, and beam energy E^*_{beam}, all in the e^+e^- center-of-mass (c.m.) frame. We require M_{bc} to be in the range $[5.27, 5.29]$ GeV/c^2, which is $\pm 3\sigma$ in resolution around the known B mass [6]. We require ΔE to be in the range $[-0.13, 0.15]$ GeV to suppress partially reconstructed $B^\pm \to D^* h^\pm$ decays, which have negative ΔE.

Most remaining backgrounds arise from continuum events, in which final-state particles are highly boosted into two jets that are approximately back-to-back in the c.m. frame. Since $B\overline{B}$ pairs are produced slightly above kinematic threshold, their final-state particles are isotropically distributed in the c.m. frame. We use boosted decision trees (BDTs) to suppress candidates from continuum events. We train them on equal numbers of simulated signal and continuum events using variables that are uncorrelated with ΔE. The simulation of these variables is verified by inspection of the flavor-specific channel. The variables used are modified Fox-Wolfram moments [34, 35]; the cosine of the polar angle of the B momentum in the c.m. frame; the absolute value of the cosine of the angle between the thrust axis of the B and the thrust axis of the rest of the charged particles and photons in the event (ROE); the longitudinal distance between the B vertex and the ROE vertex; and the output of a B-flavor-tagging algorithm [36, 37]. The thrust axis of a group of particles is the direction that maximizes the sum of the projections of the particle momenta onto it. The BDT classifier output, $\mathcal{C}$, is in the range $[0, 1]$, peaking at zero for continuum background and at one for signal. We require $\mathcal{C} > 0.15$, which retains 95% of signal in Belle data and 97% in Belle II data, while rejecting 60% and 63% of background, respectively.

To suppress D decays from $D^* \to D\pi$ arising from $e^+e^- \to c\bar{c} \to D^*\overline{D}^{(*)}X$ processes, we use the observed difference between the mass of the D candidate and the mass of the D^* candidates reconstructed by associating to the D any $\pi^\pm$ or π^0 in the ROE. We require that the differences all be outside $\pm 3\sigma$ in resolution from the known D^*-D mass difference [6]; the excluded ranges are [143.4, 147.5] MeV/c^2 and [143.8, 147.0] MeV/c^2 in Belle and Belle II data for $D^{*\pm}$, respectively, and [140.0, 145.0] MeV/c^2 in both experiments for D^{*0}. This retains 97% of signal candidates and rejects 13% of background candidates in Belle data and 18% in Belle II data. For $B^\pm \to D(\to K^\pm\pi^\mp)\pi^\pm$, we require that the dipion mass not be in the range $[3.08, 3.14]$ GeV/c^2 to veto candidates reconstructed from $B^\pm \to J/\psi(\to \ell^+\ell^-)K^\pm$ decays in which both leptons are misidentified. The ΔE distribution of such events peaks in the signal region.

In events with multiple B candidates, 2% of events for the CP-even mode and 7% for the CP-odd mode, we retain the candidate with the smallest χ^2 calculated from the reconstructed D mass, $M_{\rm bc}$ and their resolutions; for decays with D_{CP-}, the reconstructed π^0 mass and its resolution are also used in the χ^2 calculation. This selects the correct signal candidate in 70%–80% of such events in simulation.

4 Fits to data

The final event sample consists of signal, cross-feed background that comes from mis-identifying the $h^\pm$ of a signal event, other $B\overline{B}$ background sources, and continuum background. To determine the numbers of signal decays, we fit to the distributions of ΔE and $\mathcal{C}$, the variables that best discriminate between signal and the remaining background. To make $\mathcal{C}$ easier to model, we transform it to $\mathcal{C}'$ using an ordered list of $\mathcal{C}$ values from the signal simulation sample such that $\mathcal{C}'$ is the fraction of signal events present below a given value of $\mathcal{C}$ in the list. The $\mathcal{C}'$ variable is distributed uniformly in $[0, 1]$ for signal and peaks at zero for continuum background. We perform an unbinned extended maximum-likelihood fit to candidates with $\Delta E \in [-0.13, 0.14]$ GeV and $\mathcal{C}'$ in its full range.

Simulation shows that ΔE–$\mathcal{C}'$ correlations in the distributions of candidates from all sample components are negligible, and thus we factorize the two-dimensional probability density function (PDF) for each component in the fit. For each decay mode, we divide the data into 12 subsets defined by the product of the two possible electric charges of the B, the three possible D final states (two CP-specific and one flavor-specific), and whether $h^\pm$ is identified as a kaon or pion. The fit models are mostly common in all decay modes and data subsets, but the shape parameters are different in each.

For signal, the ΔE PDF is the sum of two Gaussian functions and an asymmetric Gaussian function, with all parameters fixed from simulated data except for the common mean of all three D decay modes and a common multiplier for all signal widths. These parameters are determined by the fit and account for differences in resolution between the experimental and simulated data. The $\mathcal{C}'$ PDF is a straight line with its slope fixed to the value fitted in the simulated data, except for the PDF used for the Belle $D\pi$ data, in which the slope is a free parameter.

The cross-feed ΔE PDF is same as the signal one, but with its own set of parameters. When determining the fixed parameters of the cross-feed PDF for $D\pi$, the simulated data are corrected for momentum-dependent differences in particle misidentification rates between the experimental and simulated data. Without this correction, the cross-feed ΔE PDF requires a large signal-width multiplier ($f = 1.16 \pm 0.02$) to adequately model the peak in the Belle data. To account for potential biases due to a mismodelling of the cross-feed peak, we assess a systematic uncertainty in section 5 by considering the difference between the results of the fits with and without the correction. The $\mathcal{C}'$ PDF is the sum of a straight line and an exponential function, with parameters fixed from the simulated samples.

For the $B\overline{B}$ background component, the ΔE PDF is the sum of an exponential function and a uniform distribution for the *CP* modes, and the sum of an exponential function and a Novosibirsk function [38] for the flavor-specific mode. The $\mathcal{C}'$ PDF is a straight line whose slope is fixed from simulated data.

A peaking background study has been performed for all final states. There is no sizeable peaking background found for $D_{CP+}\pi$, $D_{CP-}\pi$, $D_{CP-}K$, $D_{\rm flav}\pi$ and $D_{\rm flav}K$ modes. While for the $D_{CP+}K$ mode we see a significant peaking structure from events in which a B decays directly to KKK and estimate its yield in the signal ΔE region to be 132 ± 17 events in Belle data and 24 ± 4 in Belle II data.

These yields are estimated by linearly extrapolating the results obtained in eight D mass sidebands in data, as discussed in appendix B. The procedure is validated using simulated samples generated according to the $B^+ \to K^+K^-K^+$ results obtained in ref. [39]. Figure 8 shows a comparison of the D-mass-sideband distributions obtained from data and simulated samples. We observe good agreement, which validates our method to estimate the peaking background. In the final fit, the PDF shape of peaking background is fixed from a simulated sample.

For the continuum component, the ΔE PDF is a straight line and the $\mathcal{C}'$ PDF is the sum of two exponential functions. The larger exponential component has its parameter fixed to the value fit from simulated data, and the other is free to vary, which accounts for differences between the distributions in experimental and simulated data.

We perform a simultaneous fit to all decay modes in both the Belle and Belle II data, to determine the six charge asymmetries and three branching-fraction ratios. The yields of $B^\pm \to Dh^\pm$ with the D decaying to the state X and the charged hadron identified as $h'^\pm$, denoted as $Y_{h'}(B^\pm \to D_X h^\pm)$, are related to these physical observables via

$$Y_\pi(B^\pm \to D_X K^\pm) = \frac{1}{2}[1 \mp \mathcal{A}(B \to D_X K)]\, N(B \to D_X \pi)\, R_X\, \delta\, (1 - \varepsilon_\pm), \tag{4.1}$$

$$Y_K(B^\pm \to D_X K^\pm) = \frac{1}{2}[1 \mp \mathcal{A}(B \to D_X K)]\, N(B \to D_X \pi)\, R_X\, \delta\, \varepsilon_\pm, \tag{4.2}$$

$$Y_\pi(B^\pm \to D_X \pi^\pm) = \frac{1}{2}[1 \mp \mathcal{A}(B \to D_X \pi)]\, N(B \to D_X \pi)\, (1 - \kappa_\pm), \tag{4.3}$$

$$Y_K(B^\pm \to D_X \pi^\pm) = \frac{1}{2}[1 \mp \mathcal{A}(B \to D_X \pi)]\, N(B \to D_X \pi)\, \kappa_\pm, \tag{4.4}$$

where $\mathcal{A}$ is the charge asymmetry, R_X is the ratio between the branching-fraction of $B^\pm \to D_X K^\pm$ and $B^\pm \to D_X \pi^\pm$ for D decaying to final state X. N is the total number of events regardless of how the charged hadron was identified and of its sign, $\varepsilon_\pm$ is the efficiency to identify a kaon with ± 1 charge, and $\kappa_\pm$ is the rate for misidentifying a pion as a kaon with ± 1 charge. The efficiency δ for reconstructing $B^\pm \to DK^\pm$ relative to that for $B^\pm \to D\pi^\pm$ is independent of the D final state and equals 0.975 in Belle data and 1.000 in Belle II data. We measure PID efficiencies and misidentification rates using control samples. For Belle, we measure $\kappa_+ = 7.7\%$, $\kappa_- = 8.2\%$, $\varepsilon_+ = 83.4\%$, and $\varepsilon_- = 84.3\%$ [40]. For Belle II, we measure $\kappa_+ = 7.2\%$, $\kappa_- = 8.7\%$, $\varepsilon_+ = 79.6\%$, and $\varepsilon_- = 78.9\%$. Uncertainties on those values are typically 0.5%.

The signal yields N are independent for the Belle and Belle II data. For each background component, separate yields are fitted for B^+ and B^- to account for their possible charge asymmetries.

To check for fit biases, we perform the fit on five independent sets of simulated data. We also repeat the analysis on 1000 data sets simulated according to the fit model for seven different values of $\mathcal{A}_{CP\pm}$: 0, ± 0.1, ± 0.2, ± 0.3. In all cases, the fit results are consistent with the input values.

5 Systematic uncertainties

We consider several sources of systematic uncertainties, which are summarized in table 1. In general, for parameters fixed in the fits, we repeat the fits with the parameter varied by its uncertainty and take the resulting change in our results as the fit-model systematic uncertainty. We do this for the fixed PDFs parameters, PID efficiencies and mis-identification rates, peaking background yields, and the efficiency ratio. We ignore correlations between those uncertainties and combine them by adding them in quadrature. The peaking background estimation is obtained directly from the data using D mass sidebands. This provides the largest systematic uncertainty and is due to the uncertainty on the peaking background contamination which is statistical in nature and will improve with larger sample size. We also assign systematic uncertainties (included in the "PDFs parameters" item of table 1) from the difference between correcting and not correcting for the momentum-dependent pion misidentification rates when modeling the cross-feed PDFs for the $D\pi$ data, and having common and independent mode parameters for the ΔE PDFs for DK and $D\pi$. We use a common mean for the signal ΔE PDFs for all modes. The corresponding systematic uncertainty ("Signal-ΔE common mean" item of table 1) is estimated from the variations resulting from assigning different mean

	$\mathcal{R}_{CP+}$	$\mathcal{R}_{CP-}$	$\mathcal{A}_{CP+}$	$\mathcal{A}_{CP-}$
PDFs parameters	0.012	0.014	0.002	0.002
PID parameters	0.009	0.010	0.003	0.005
Peaking background yields	0.033	0.002	0.013	—
Efficiency ratio	0.001	0.001	< 0.001	< 0.001
Signal-ΔE common mean	0.005	0.006	< 0.001	< 0.001
Total systematic uncertainty	0.036	0.019	0.014	0.006
Statistical uncertainty	0.081	0.074	0.058	0.057

Table 1. Systematic and statistical uncertainties.

D_X mode		$N(B \to D_X K)$	$N(B \to D_X \pi)$
$D \to K^{\pm}\pi^{\mp}$	Belle	4238 ± 94	59481 ± 267
	Belle II	1084 ± 44	14229 ± 126
$D \to K^+K^-$	Belle	476 ± 36	5559 ± 85
	Belle II	107 ± 15	1336 ± 40
$D \to K_S^0\pi^0$	Belle	541 ± 42	6484 ± 95
	Belle II	145 ± 16	1763 ± 46

Table 2. Signal yields extracted from the simultaneous fit in data.

values to the ΔE PDFs, i.e., $B \to D_X K$ and $B \to D_X \pi$ with the same or independent means, B^- and B^+ with the same or independent means. For the slopes of the $\mathcal{C}'$ PDFs of the $B\overline{B}$ component, we calculate the systematic uncertainty from the maximum difference among fit results in which the slope is taken from simulation, as in the nominal fit, or taken from the signal $\mathcal{C}'$ PDFs slope in data, or determined by the fit itself.

6 Results

Figures 1, 3, and 5 show distributions and the fit results for candidates satisfying $|\Delta E| < 0.05$ GeV and $0.65 < \mathcal{C}' < 1.0$ for Belle data; figures 2, 4, and 6 show the corresponding plots for Belle II data. The fit results agree with the data; the small shifts seen for $B \to D_X \pi$ signal in ΔE are accounted for in the systematic uncertainty estimation. The data-fit discrepancy observed in the ΔE projection for $B^+ \to D(\to K^+K^-)K^+$ in the Belle sample (figure 3(e)) is interpreted as a statistical fluctuation since no mismodelling is observed in the $\mathcal{C}'$ projection (figure 3(g)) nor in those for $B^- \to D(\to K^-K^+)K^-$ (figure 3(f) and (h)). Table 2 summarizes the signal yields.

JHEP05(2024)212

	68.3% CL	95.4% CL
	[8.5, 16.5]	[5.0, 22.0]
ϕ_3 (°)	[84.5, 95.5]	[80.0, 100.0]
	[163.3, 171.5]	[157.5, 175.0]
r_B	[0.321, 0.465]	[0.241, 0.522]

Table 3. One-dimensional 68.3% and 95.4% CL regions for ϕ_3 and r_B, for $\phi_3 \in [0^\circ, 180^\circ]$.

From the combined Belle and Belle II data, the ratios of branching-fraction ratios and *CP* asymmetries of $B^\pm \to D_{CP}K^\pm$ are

$$\mathcal{R}_{CP+} = 1.164 \pm 0.081 \pm 0.036, \tag{6.1}$$

$$\mathcal{R}_{CP-} = 1.151 \pm 0.074 \pm 0.019, \tag{6.2}$$

$$\mathcal{A}_{CP+} = (+12.5 \pm 5.8 \pm 1.4)\%, \tag{6.3}$$

$$\mathcal{A}_{CP-} = (-16.7 \pm 5.7 \pm 0.6)\%, \tag{6.4}$$

where the first uncertainty is statistical and the second is systematic.

The significances of *CP* violation for *CP*-even and *CP*-odd D final states are approximated using $\sqrt{-2\ln(\mathcal{L}_0/\mathcal{L}_{\rm max})}\,\sigma_{\rm stat}/\sqrt{\sigma^2_{\rm stat}+\sigma^2_{\rm syst}}$, where $\mathcal{L}_{\rm max}$ is the maximum likelihood value, $\mathcal{L}_0$ is the likelihood value obtained assuming *CP* symmetry, and σ are the statistical and systematic uncertainties. We find 2.0σ and 2.8σ significances for *CP* violation in the D_{CP+} and D_{CP-} modes, respectively. This corresponds to 3.5σ evidence for the asymmetries being different, i.e., $\mathcal{A}_{CP+} \neq \mathcal{A}_{CP-}$. The measured $\mathcal{R}_{CP+}$ value is 2.2σ away from its expectation as estimated from the world-average values [6, 7] of ϕ_3, r_B, and δ_B, while the measured $\mathcal{R}_{CP-}$ value agrees well with its expected value. An underestimation of the peaking-background yield for $D_{CP+}K$ could be a possible explanation, but this estimation is carefully done using eight different sidebands in data as described in section 4 and appendix B. Fit bias is also excluded here; we examine data both from realistic simulation and simulation based on the fit model and find no bias (section 4). The *CP* asymmetries of $B^\pm \to D_X\pi^\pm$ and $B^\pm \to D_{\rm flav}K^\pm$ are $\mathcal{A}^\pi_{CP+} = (-2.0 \pm 1.4 \pm 0.2)\%$, $\mathcal{A}^\pi_{CP-} = (-0.3 \pm 1.2 \pm 0.2)\%$, $\mathcal{A}^\pi_{\rm flav} = (-0.5 \pm 0.4 \pm 0.2)\%$, and $\mathcal{A}^K_{\rm flav} = (-1.4 \pm 1.7 \pm 0.1)\%$, consistent with the negligible *CP* asymmetries in these modes.

With these results for $R_{CP\pm}$ and $\mathcal{A}_{CP\pm}$, we constrain the angle ϕ_3 using a frequentist approach as implemented in the CkmFitter package [41]. Figure 7 shows the resulting distributions of the p-value (the complement of the confidence level, $1-$ CL). Given the $\delta_B \leftrightarrow \phi_3$ symmetry of equations 1.6 and 1.7, the distribution for δ_B is identical to that for ϕ_3. Table 3 lists the 68.3%- and 95.4%-CL intervals for ϕ_3 and r_B for solutions with $\phi_3 \in [0^\circ, 180^\circ]$. The large value measured for $\mathcal{R}_{CP+}$ results in a relatively large r_B which, in turn, gives a more stringent constraint that expected on ϕ_3 due to the correlation between r_B and ϕ_3. The p-value of the agreement of our result of (ϕ_3, r_B, δ_B) with the world average values is calculated to be 4% from analysing an ensemble of 100,000 pseudo-experiments.

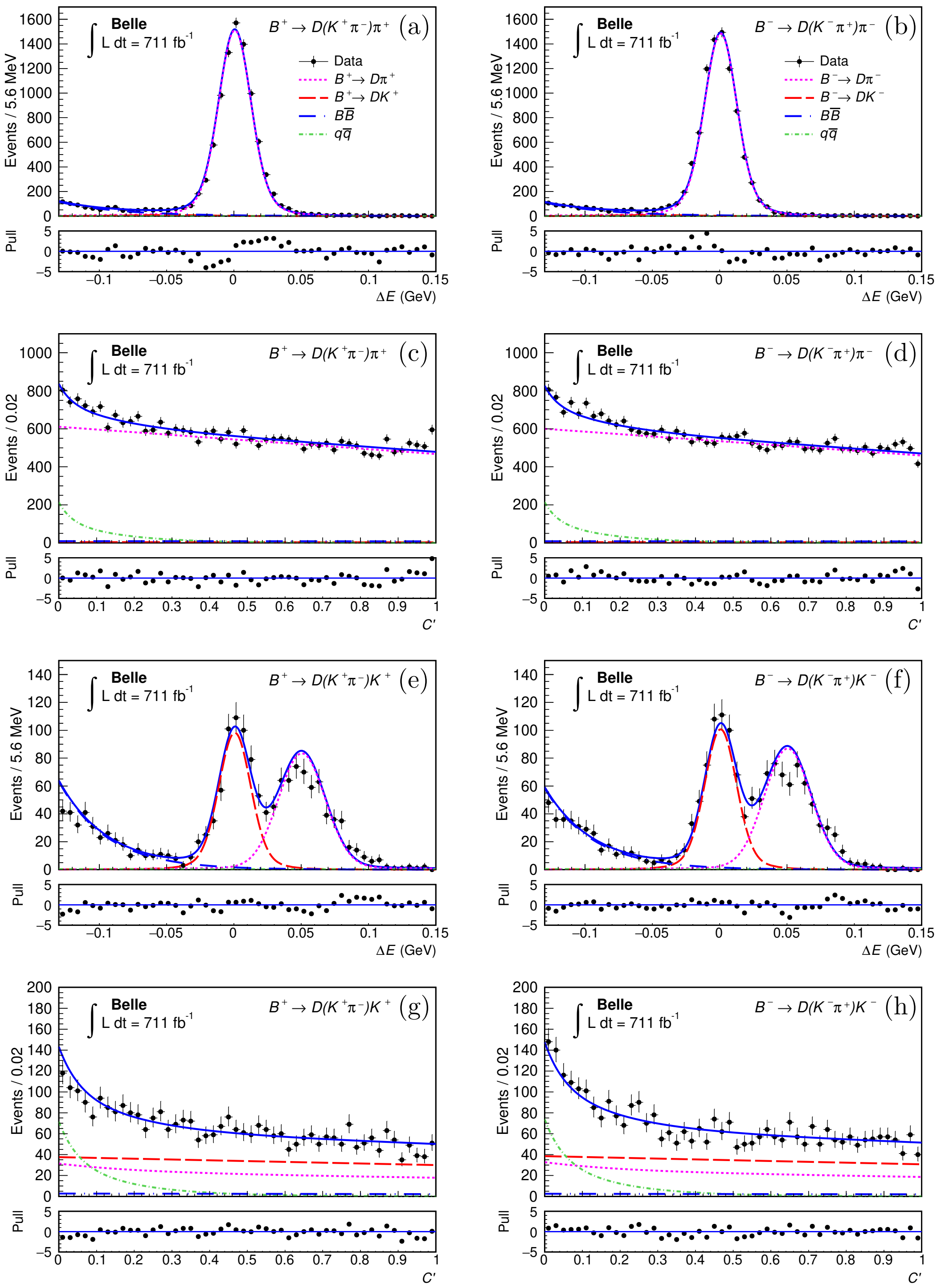

Figure 1. Distributions of ΔE and $\mathcal{C}'$ for $B^{\pm} \to D(\to K^{\pm}\pi^{\mp})h^{\pm}$ candidates in the Belle data with fit projections overlaid. Differences between data and fit results normalized by the uncertainty in data are shown in the bottom panels.

JHEP05(2024)212

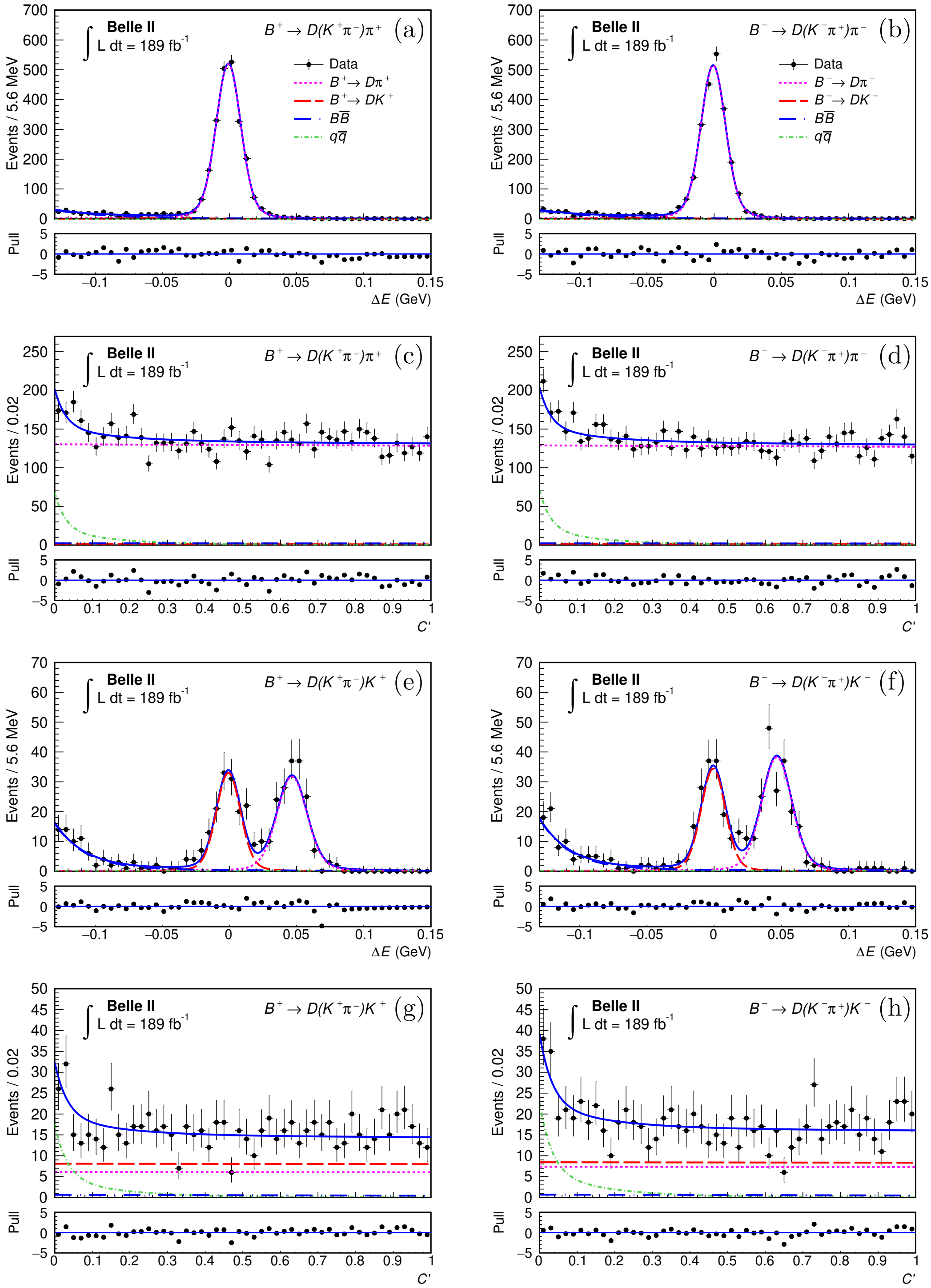

Figure 2. Distributions of ΔE and $\mathcal{C}'$ for $B^{\pm} \to D(\to K^{\pm}\pi^{\mp})h^{\pm}$ candidates in the Belle II data with fit projections overlaid. Differences between data and fit results normalized by the uncertainty in data are shown in the bottom panels.

JHEP05(2024)212

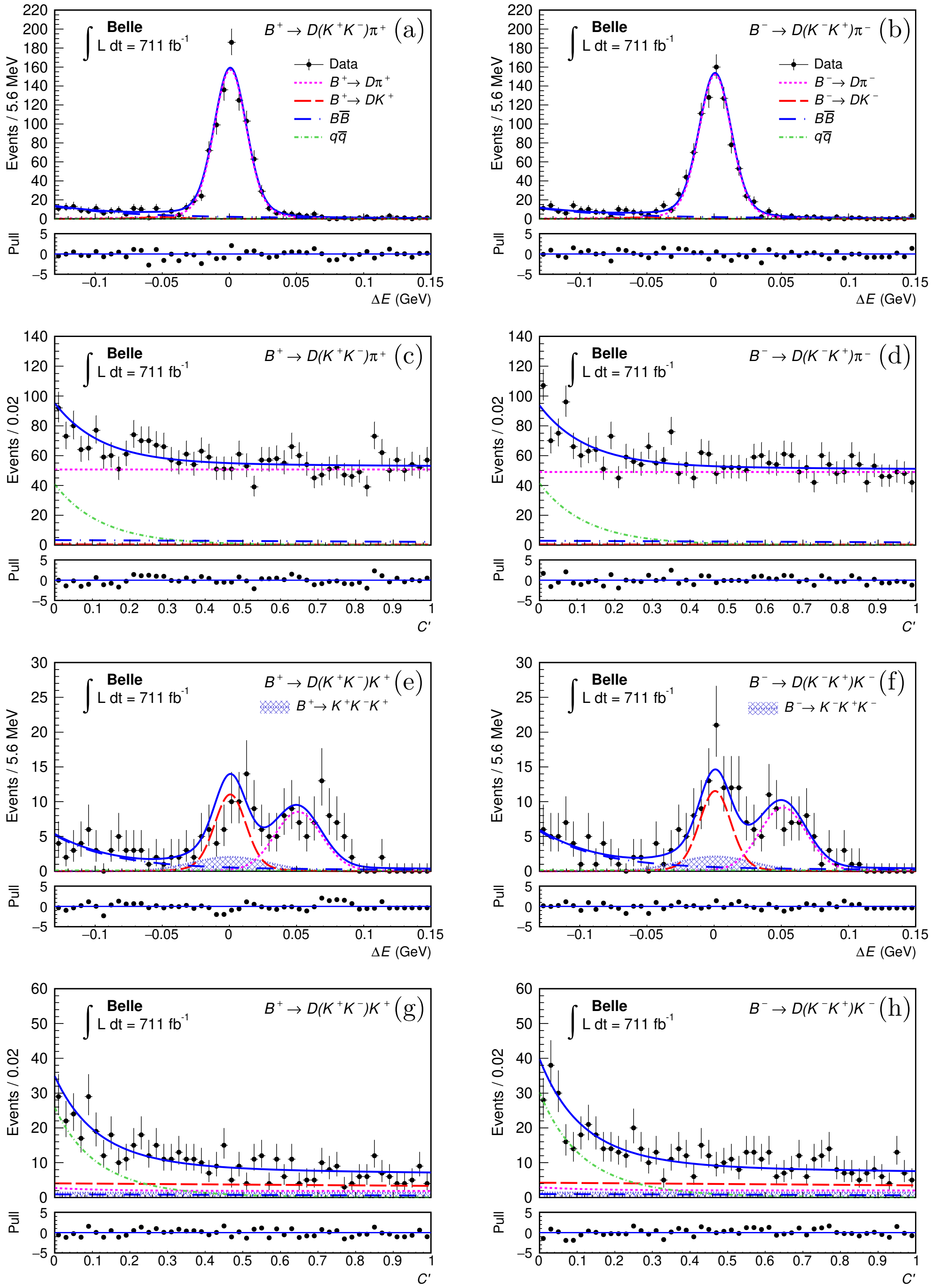

Figure 3. Distributions of ΔE and $\mathcal{C}'$ for $B^{\pm} \to D(\to K^+K^-)h^{\pm}$ candidates in the Belle data with fit projections overlaid. Differences between data and fit results normalized by the uncertainty in data are shown in the bottom panels.

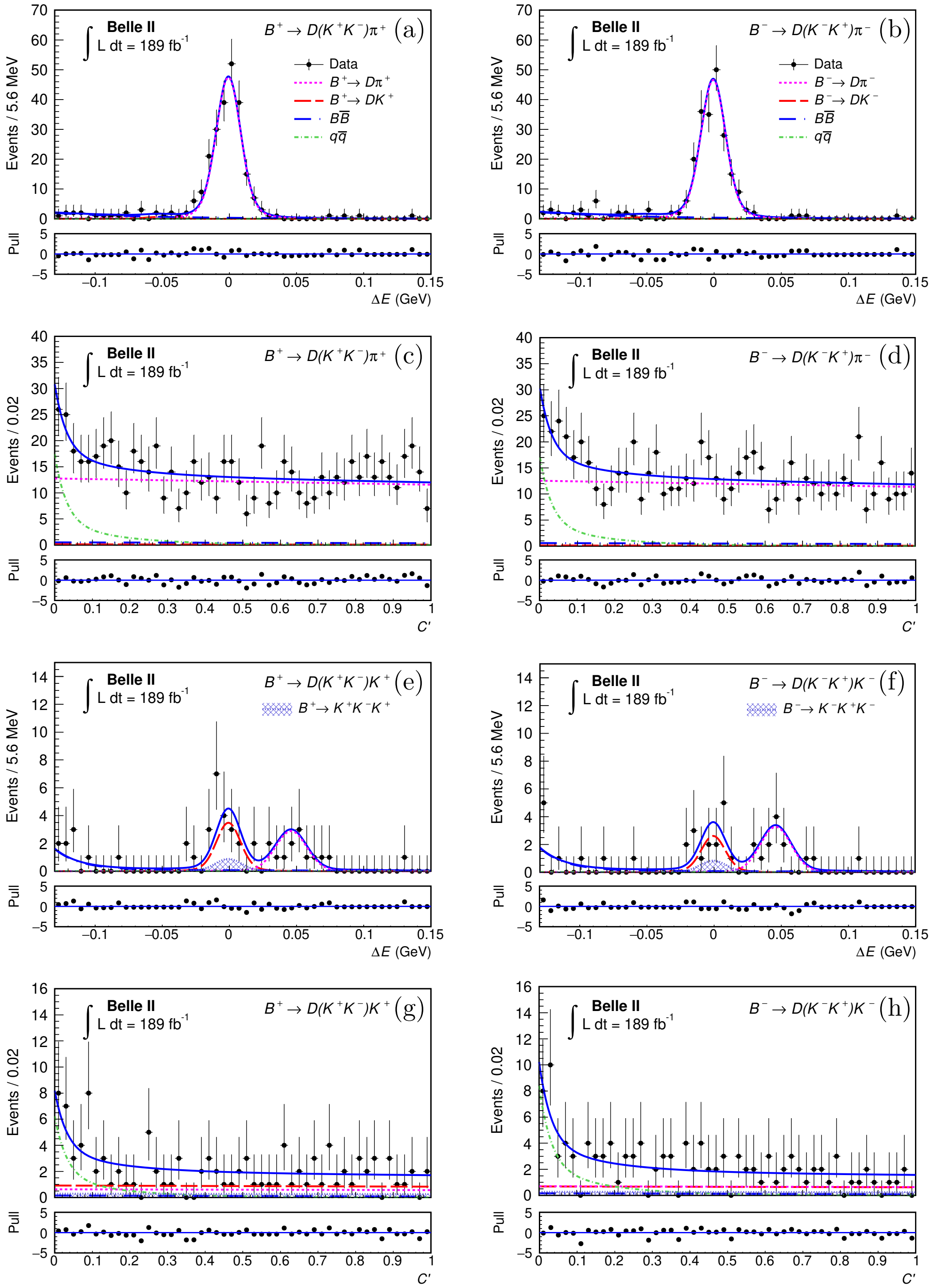

Figure 4. Distributions of ΔE and $\mathcal{C}'$ for $B^{\pm} \to D(\to K^+K^-)h^{\pm}$ candidates in the Belle II data with fit projections overlaid. Differences between data and fit results normalized by the uncertainty in data are shown in the bottom panels.

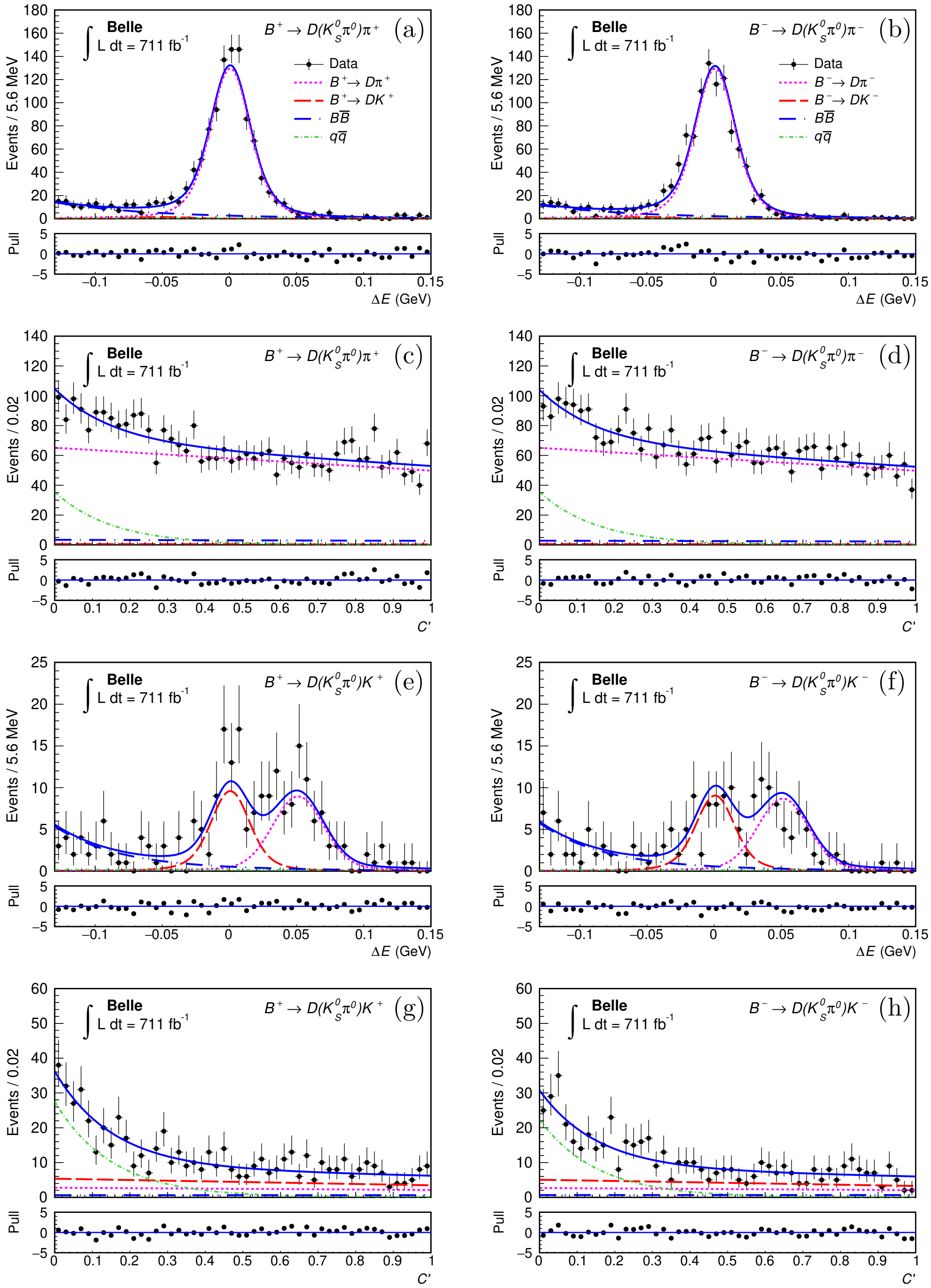

Figure 5. Distributions of ΔE and $\mathcal{C}'$ for $B^{\pm} \to D(\to K_S^0\pi^0)h^{\pm}$ candidates in the Belle data with fit projections overlaid. Differences between data and fit results normalized by the uncertainty in data are shown in the bottom panels.

JHEP05(2024)212

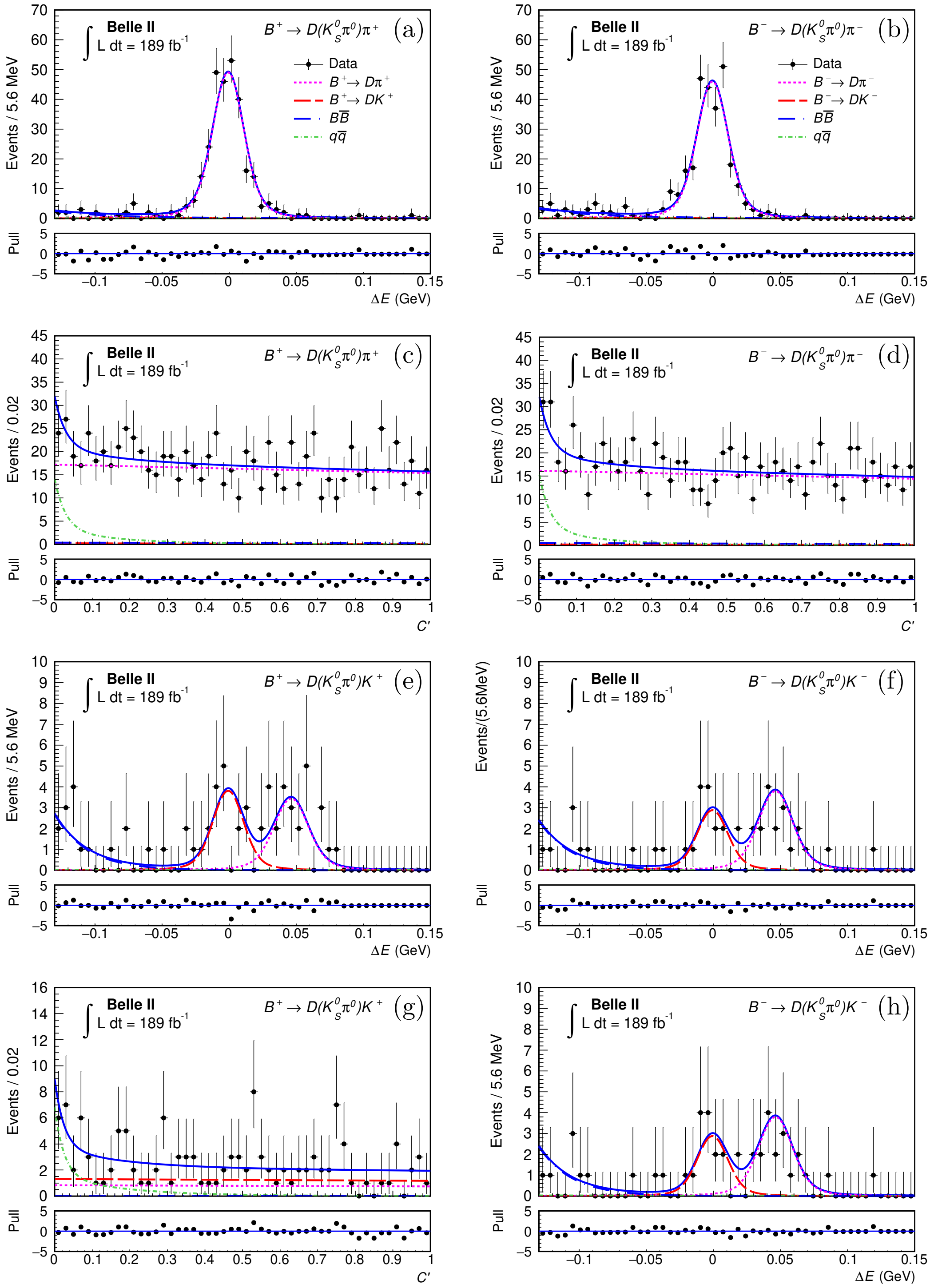

Figure 6. Distributions of ΔE and $\mathcal{C}'$ for $B^{\pm} \to D(\to K_S^0 \pi^0)h^{\pm}$ candidates in the Belle II data with fit projections overlaid. Differences between data and fit results normalized by the uncertainty in data are shown in the bottom panels.

JHEP05(2024)212

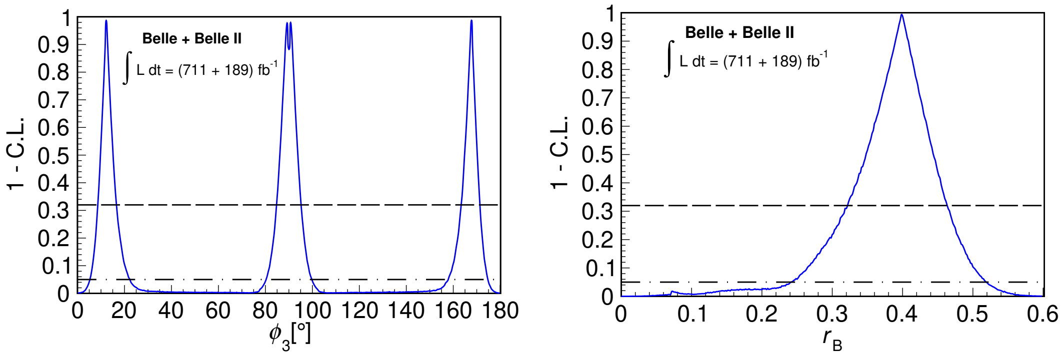

Figure 7. p-values $(1 - \mathrm{CL})$ as functions of ϕ_3 (left) and r_B (right). The dashed horizontal line shows the 68.3% CL, and the dash-dotted line shows the 95.4% CL.

	$\mathcal{R}_{CP+}$	$\mathcal{R}_{CP-}$	$\mathcal{A}_{CP+}$	$\mathcal{A}_{CP-}$
$\mathcal{R}_{CP+}$	1	−0.081	0.060	0.000
$\mathcal{R}_{CP-}$		1	0.000	0.056
$\mathcal{A}_{CP+}$			1	0.000
$\mathcal{A}_{CP-}$				1

Table 4. Statistical correlation matrix of measured observables.

7 Conclusion

We measure the *CP* asymmetries and ratios of branching-fraction ratios for $B^{\pm} \to D_{CP\pm}K^{\pm}$ for the *CP*-even D final state K^+K^- and the *CP*-odd final state $K_S^0\pi^0$ with a combined analysis of the full Belle data set of 772×10^6 $B\bar{B}$ pairs and a Belle II data set containing 198×10^6 $B\bar{B}$ pairs. As expected, the asymmetries have opposite signs, showing prominent *CP* violation in $B^{\pm} \to D_{CP}K^{\pm}$. The statistical and systematic precision of our results, based on a data set almost four times larger than the previous Belle measurement [15], is significantly improved. The results are consistent with those of the *BABAR* and LHCb experiments [42, 43]. We obtain 68.3%-CL intervals for the CKM angle ϕ_3 and the amplitude ratio r_B:

$$\phi_3 \in [8.5^\circ, 16.5^\circ] \cup [84.5^\circ, 95.5^\circ] \cup [163.3^\circ, 171.5^\circ], \tag{7.1}$$

$$r_B \in [0.321, 0.465]. \tag{7.2}$$

A Correlation matrices

Table 4 and 5 list the statistical and systematic correlation matrices for $\mathcal{A}_{CP\pm}$ and $\mathcal{R}_{CP\pm}$. We vary every fixed parameter randomly by Gaussian distribution for thousand times. We repeat the fit with the varied values for every fixed parameter, which can result in Gaussian-like distributions of the measured observables. The correlations are calculated by using those Gaussian-like distributions. These correlation matrices are used in the extraction of ϕ_3, δ_B and r_B.

JHEP05(2024)212

	$\mathcal{R}_{CP+}$	$\mathcal{R}_{CP-}$	$\mathcal{A}_{CP+}$	$\mathcal{A}_{CP-}$
$\mathcal{R}_{CP+}$	1	−0.063	0.342	0.005
$\mathcal{R}_{CP-}$		1	−0.128	−0.490
$\mathcal{A}_{CP+}$			1	0.542
$\mathcal{A}_{CP-}$				1

Table 5. Systematic correlation matrix of measured observables.

Analysis	Lower sidebands	Upper sidebands
Belle	[1.67,1.71][1.71,1.75]	[1.90,1.94][1.94,1.98]
	[1.75,1.79][1.79,1.83]	[1.98,2.02][2.02,2.06]
Belle II	[1.706,1.732][1.732,1.758]	[1.758,1.784][1.784,1.810]
	[1.920,1.946][1.946,1.972]	[1.972,1.998][1.998,2.024]

Table 6. D sideband mass regions for D_{CP+} mode, in GeV/c^2 units.

B D mass sidebands for the $B^{\pm} \to D_{CP+}K^{\pm}$ mode

In section 4, we use eight D mass sidebands of data to estimate the peaking background for the D_{CP+} mode. Table 6 lists the sideband mass ranges used in the Belle and Belle II analyses, respectively. These sidebands are chosen to extend over the same range as the signal D region.

The sideband procedure is validated by comparing the results in the data and in the simulated samples, as illustrated in figure 8, showing a good agreement for all sidebands.

Figure 9 shows distributions and fit-result projections in the data sidebands for the Belle analysis. We obtain the peaking background yield for each sideband and interpolate those yields linearly.

The Belle II data sample used in this analysis has only an integrated luminosity of 189 fb^{-1}, which is insufficient to estimate the yield of peaking background. Instead we obtain the Belle II yield by scaling the Belle yield by the reconstruction efficiencies ϵ of $B^- \to K^-K^+K^-$ in simulated data and the luminosities (L) of Belle and Belle II data samples:

$$Y_{B2}(B^- \to K^-K^+K^-) = Y_B(B^- \to K^-K^+K^-)\frac{\epsilon_{B2}L_{B2}}{\epsilon_B L_B}, \tag{B.1}$$

where subscripts B and $B2$ stand for Belle and Belle II, respectively.

Acknowledgments

This work, based on data collected using the Belle II detector, which was built and commissioned prior to March 2019, was supported by Higher Education and Science Committee of the Republic of Armenia Grant No. 23LCG-1C011; Australian Research Council and Research Grants No. DP200101792, No. DP210101900, No. DP210102831, No. DE220100462, No. LE210100098, and No. LE230100085; Austrian Federal Ministry of Education, Science and Research, Austrian Science Fund No. P 31361-N36 and No. J4625-N, and Horizon

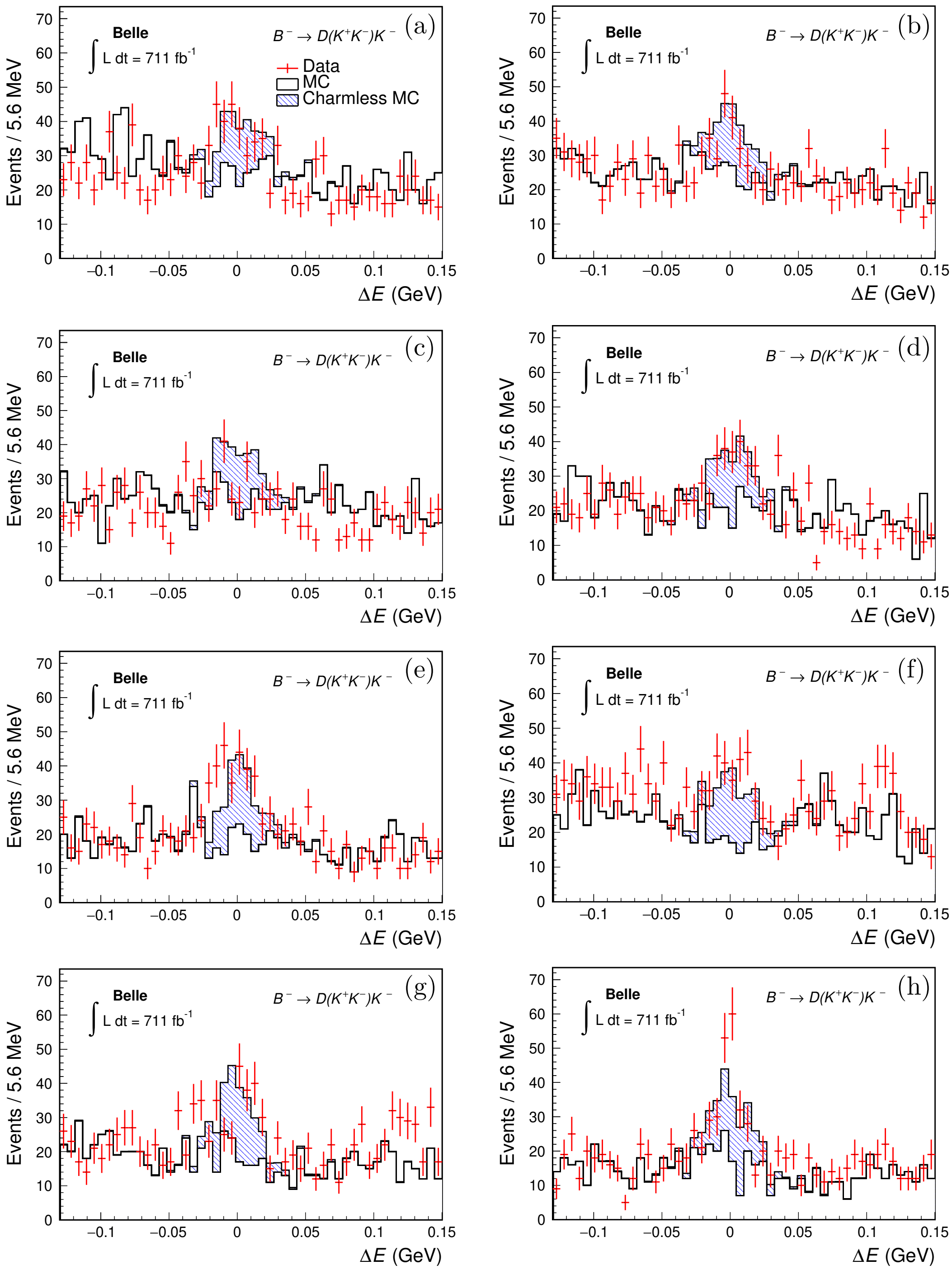

Figure 8. ΔE distributions of $B^{\pm} \to D(\to K^- K^+)K^{\pm}$ in Belle data and Belle simulated samples for the lower sidebands [1.67, 1.71] GeV/c^2 (a), [1.71, 1.75] GeV/c^2 (b), [1.75, 1.79] GeV/c^2 (c), and [1.79, 1.83] GeV/c^2 (d), and the upper sidebands [1.90, 1.94] GeV/c^2 (e), [1.94, 1.98] GeV/c^2 (f), [1.98, 2.02] GeV/c^2 (g), and [2.02, 2.06] GeV/c^2 (h). The red error bar is Belle data, empty histogram stands for Belle simulated sample (without charmless decays of B mesons), the filled blue histogram stands for charmless-only decays of B in Belle simulated sample.

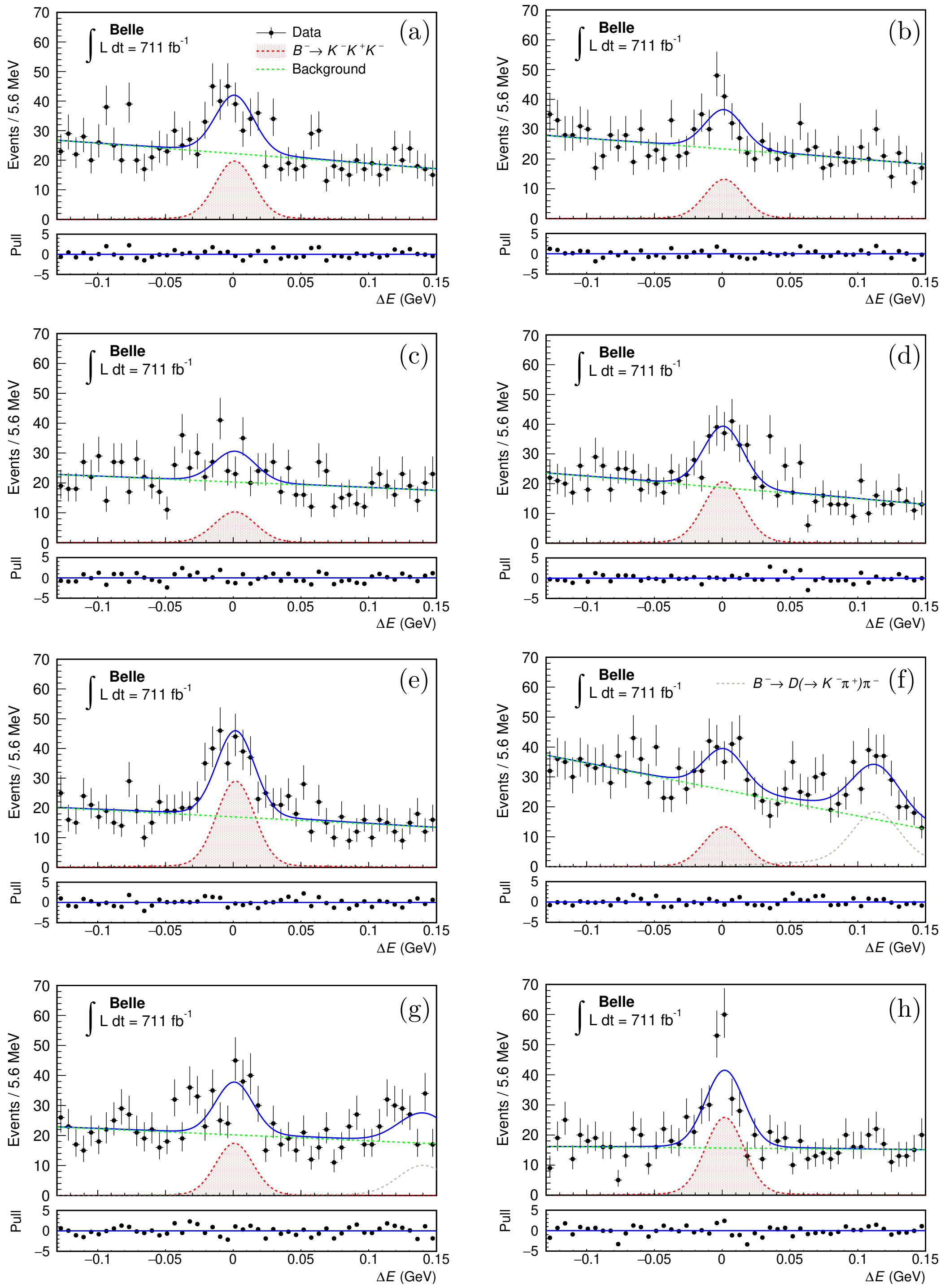

Figure 9. ΔE distributions of $B^\pm \to D(\to K^- K^+)K^\pm$ in Belle data with the fit projections overlaid for the lower sidebands [1.67, 1.71] GeV/c^2 (a), [1.71, 1.75] GeV/c^2 (b), [1.75, 1.79] GeV/c^2 (c), and [1.79, 1.83] GeV/c^2 (d), and the upper sidebands [1.90, 1.94] GeV/c^2 (e), [1.94, 1.98] GeV/c^2 (f), [1.98, 2.02] GeV/c^2 (g), and [2.02, 2.06] GeV/c^2 (h). The grey dashed line in (f) and (g) indicates the peaking structure of $B^\pm \to D(\to K^\pm\pi^\mp)\pi^\pm$ when the two pions are misidentified as kaons.

JHEP05(2024)212

2020 ERC Starting Grant No. 947006 "InterLeptons"; Natural Sciences and Engineering Research Council of Canada, Compute Canada and CANARIE; National Key R&D Program of China under Contract No. 2022YFA1601903, National Natural Science Foundation of China and Research Grants No. 11575017, No. 11761141009, No. 11705209, No. 11975076, No. 12135005, No. 12150004, No. 12161141008, and No. 12175041, and Shandong Provincial Natural Science Foundation Project ZR2022JQ02; the Czech Science Foundation Grant No. 22-18469S; European Research Council, Seventh Framework PIEF-GA-2013-622527, Horizon 2020 ERC-Advanced Grants No. 267104 and No. 884719, Horizon 2020 ERC-Consolidator Grant No. 819127, Horizon 2020 Marie Sklodowska-Curie Grant Agreement No. 700525 "NIOBE" and No. 101026516, and Horizon 2020 Marie Sklodowska-Curie RISE project JENNIFER2 Grant Agreement No. 822070 (European grants); L'Institut National de Physique Nucléaire et de Physique des Particules (IN2P3) du CNRS and L'Agence Nationale de la Recherche (ANR) under grant ANR-21-CE31-0009 (France); BMBF, DFG, HGF, MPG, and AvH Foundation (Germany); Department of Atomic Energy under Project Identification No. RTI 4002, Department of Science and Technology, and UPES SEED funding programs No. UPES/R&D-SEED-INFRA/17052023/01 and No. UPES/R&D-SOE/20062022/06 (India); Israel Science Foundation Grant No. 2476/17, U.S.-Israel Binational Science Foundation Grant No. 2016113, and Israel Ministry of Science Grant No. 3-16543; Istituto Nazionale di Fisica Nucleare and the Research Grants BELLE2; Japan Society for the Promotion of Science, Grant-in-Aid for Scientific Research Grants No. 16H03968, No. 16H03993, No. 16H06492, No. 16K05323, No. 17H01133, No. 17H05405, No. 18K03621, No. 18H03710, No. 18H05226, No. 19H00682, No. 20H05850, No. 20H05858, No. 22H00144, No. 22K14056, No. 22K21347, No. 23H05433, No. 26220706, and No. 26400255, the National Institute of Informatics, and Science Information NETwork 5 (SINET5), and the Ministry of Education, Culture, Sports, Science, and Technology (MEXT) of Japan; National Research Foundation (NRF) of Korea Grants No. 2016R1D1A1B02012900, No. 2018R1A2B3003643, No. 2018R1A6A1A06024970, No. 2019R1I1A3A01058933, No. 2021R1A6A1A03043957, No. 2021R1F1A1060423, No. 2021R1F1A1064008, No. 2022R1A2C1003993, and No. RS-2022-00197659, Radiation Science Research Institute, Foreign Large-Size Research Facility Application Supporting project, the Global Science Experimental Data Hub Center of the Korea Institute of Science and Technology Information and KREONET/GLORIAD; Universiti Malaya RU grant, Akademi Sains Malaysia, and Ministry of Education Malaysia; Frontiers of Science Program Contracts No. FOINS-296, No. CB-221329, No. CB-236394, No. CB-254409, and No. CB-180023, and SEP-CINVESTAV Research Grant No. 237 (Mexico); the Polish Ministry of Science and Higher Education and the National Science Center; the Ministry of Science and Higher Education of the Russian Federation and the HSE University Basic Research Program, Moscow; University of Tabuk Research Grants No. S-0256-1438 and No. S-0280-1439 (Saudi Arabia); Slovenian Research Agency and Research Grants No. J1-9124 and No. P1-0135; Agencia Estatal de Investigacion, Spain Grant No. RYC2020-029875-I and Generalitat Valenciana, Spain Grant No. CIDEGENT/2018/020; National Science and Technology Council, and Ministry of Education (Taiwan); Thailand Center of Excellence in Physics; TUBITAK ULAKBIM (Turkey); National Research Foundation of Ukraine, Project No. 2020.02/0257, and Ministry of Education and Science of Ukraine; the U.S. National Science Foundation and Research

Grants No. PHY-1913789 and No. PHY-2111604, and the U.S. Department of Energy and Research Awards No. DE-AC06-76RLO1830, No. DE-SC0007983, No. DE-SC0009824, No. DE-SC0009973, No. DE-SC0010007, No. DE-SC0010073, No. DE-SC0010118, No. DE-SC0010504, No. DE-SC0011784, No. DE-SC0012704, No. DE-SC0019230, No. DE-SC0021274, No. DE-SC0021616, No. DE-SC0022350, No. DE-SC0023470; and the Vietnam Academy of Science and Technology (VAST) under Grants No. NVCC.05.12/22-23 and No. DL0000.02/24-25.

These acknowledgements are not to be interpreted as an endorsement of any statement made by any of our institutes, funding agencies, governments, or their representatives.

We thank the SuperKEKB team for delivering high-luminosity collisions; the KEK cryogenics group for the efficient operation of the detector solenoid magnet; the KEK computer group and the NII for on-site computing support and SINET6 network support; and the raw-data centers at BNL, DESY, GridKa, IN2P3, INFN, and the University of Victoria for off-site computing support.

References

[1] N. Cabibbo, *Unitary Symmetry and Leptonic Decays*, Phys. Rev. Lett. **10** (1963) 531 [INSPIRE].

[2] M. Kobayashi and T. Maskawa, *CP Violation in the Renormalizable Theory of Weak Interaction*, Prog. Theor. Phys. **49** (1973) 652 [INSPIRE].

[3] M. Gronau and D. London, *How to determine all the angles of the unitarity triangle from* $B_d^0 \to DK_S$ *and* ${B_s}^0 \to D\varphi$, Phys. Lett. B **253** (1991) 483 [INSPIRE].

[4] M. Gronau and D. Wyler, *On determining a weak phase from CP asymmetries in charged B decays*, Phys. Lett. B **265** (1991) 172 [INSPIRE].

[5] M. Rama, *Effect of D-$\bar{D}$ mixing in the extraction of* γ *with* $B^- \to D^0K^-$ *and* $B^- \to D^0\pi^-$ *decays*, Phys. Rev. D **89** (2014) 014021 [arXiv:1307.4384] [INSPIRE].

[6] Particle Data Group collaboration, *Review of Particle Physics*, PTEP **2022** (2022) 083C01 and 2023 update [INSPIRE].

[7] HFLAV collaboration, *Averages of b-hadron, c-hadron, and* τ*-lepton properties as of 2021*, Phys. Rev. D **107** (2023) 052008 [arXiv:2206.07501] [INSPIRE].

[8] LHCb collaboration, *Simultaneous determination of the CKM angle* γ *and parameters related to mixing and CP violation in the charm sector*, LHCb-CONF-2022-003.

[9] D. Atwood, I. Dunietz and A. Soni, *Enhanced CP violation with* $B \to KD^0(\bar{D}^0)$ *modes and extraction of the CKM angle* γ, Phys. Rev. Lett. **78** (1997) 3257 [hep-ph/9612433] [INSPIRE].

[10] D. Atwood, I. Dunietz and A. Soni, *Improved methods for observing CP violation in* $B^\pm \to K^\pm D$ *and measuring the CKM phase* γ, Phys. Rev. D **63** (2001) 036005 [hep-ph/0008090] [INSPIRE].

[11] Belle collaboration, *Evidence for the Suppressed Decay* $B^- \to DK^-$, $D \to K^+\pi^-$, Phys. Rev. Lett. **106** (2011) 231803 [arXiv:1103.5951] [INSPIRE].

[12] A. Giri, Y. Grossman, A. Soffer and J. Zupan, *Determining* γ *using* $B^\pm \to DK^\pm$ *with multibody D decays*, Phys. Rev. D **68** (2003) 054018 [hep-ph/0303187] [INSPIRE].

[13] A. Bondar, *Proceedings of BINP Special Analysis Meeting on Dalitz Analysis*, unpublished (2002).

[14] Belle and Belle-II collaborations, *Combined analysis of Belle and Belle II data to determine the CKM angle ϕ_3 using $B^+ \to D(K^0_S h^+ h^-)h^+$ decays*, JHEP **02** (2022) 063 [*Erratum ibid.* **12** (2022) 034] [arXiv:2110.12125] [INSPIRE].

[15] Belle collaboration, *Study of $B^\pm \to D_{CP\pm}K^\pm$ and $D^*_{CP\pm}K^\pm$ decays*, Phys. Rev. D **73** (2006) 051106 [hep-ex/0601032] [INSPIRE].

[16] S. Kurokawa and E. Kikutani, *Overview of the KEKB accelerators*, Nucl. Instrum. Meth. A **499** (2003) 1 [INSPIRE].

[17] T. Abe et al., *Achievements of KEKB*, PTEP **2013** (2013) 03A001 [INSPIRE].

[18] SuperKEKB collaboration, *SuperKEKB Collider*, Nucl. Instrum. Meth. A **907** (2018) 188 [arXiv:1809.01958] [INSPIRE].

[19] Belle collaboration, *The Belle Detector*, Nucl. Instrum. Meth. A **479** (2002) 117 [INSPIRE].

[20] Belle collaboration, *Physics Achievements from the Belle Experiment*, PTEP **2012** (2012) 04D001 [arXiv:1212.5342] [INSPIRE].

[21] H. Schenck, *Equivariant Chow cohomology of nonsimplicial toric varieties*, arXiv:1101.0352.

[22] D.J. Lange, *The EvtGen particle decay simulation package*, Nucl. Instrum. Meth. A **462** (2001) 152 [INSPIRE].

[23] B.F.L. Ward, S. Jadach and Z. Was, *Precision calculation for $e^+e^- \to 2f$: the KK MC project*, Nucl. Phys. B Proc. Suppl. **116** (2003) 73 [hep-ph/0211132] [INSPIRE].

[24] T. Sjostrand, S. Mrenna and P.Z. Skands, *A Brief Introduction to PYTHIA 8.1*, Comput. Phys. Commun. **178** (2008) 852 [arXiv:0710.3820] [INSPIRE].

[25] R. Brun et al., *GEANT3.21*, CERN-DD-EE-84-01 (1984) [INSPIRE].

[26] GEANT4 collaboration, *GEANT4–a simulation toolkit*, Nucl. Instrum. Meth. A **506** (2003) 250 [INSPIRE].

[27] E. Barberio and Z. Was, *PHOTOS: A Universal Monte Carlo for QED radiative corrections. Version 2.0*, Comput. Phys. Commun. **79** (1994) 291 [INSPIRE].

[28] Belle-II Framework Software Group collaboration, *The Belle II Core Software*, Comput. Softw. Big Sci. **3** (2019) 1 [arXiv:1809.04299] [INSPIRE].

[29] Belle II collaboration, *Belle II Analysis Software Framework (basf2)*, DOI:10.5281/zenodo.5574115.

[30] M. Gelb et al., *B2BII: Data Conversion from Belle to Belle II*, Comput. Softw. Big Sci. **2** (2018) 9 [arXiv:1810.00019] [INSPIRE].

[31] Belle-II collaboration, *Study of $B \to D^{(*)}h$ decays using* 62.8 fb^{-1} *of Belle II data*, in the proceedings of the *55th Rencontres de Moriond on QCD and High Energy Interactions*, , Italy, March 27 – April 03 (2021) [arXiv:2104.03628] [INSPIRE].

[32] H. Nakano, *Search for new physics by a time-dependent CP violation analysis of the decay $B \to K_S\eta\gamma$ using the Belle detector*, Ph.D. thesis, Tohoku University (2014), https://belle.kek.jp/belle/theses/doctor/nakano15.pdf [INSPIRE].

[33] Belle collaboration, *Measurement of time-dependent CP asymmetries in $B^0 \to K^0_S\eta\gamma$ decays*, Phys. Rev. D **97** (2018) 092003 [arXiv:1803.07774] [INSPIRE].

JHEP05(2024)212

[34] G.C. Fox and S. Wolfram, *Observables for the Analysis of Event Shapes in e^+e^- Annihilation and Other Processes*, *Phys. Rev. Lett.* **41** (1978) 1581 [INSPIRE].

[35] BELLE collaboration, *Evidence for $B^0 \to \pi^0\pi^0$*, *Phys. Rev. Lett.* **91** (2003) 261801 [hep-ex/0308040] [INSPIRE].

[36] BELLE collaboration, *Neutral B flavor tagging for the measurement of mixing induced CP violation at Belle*, *Nucl. Instrum. Meth. A* **533** (2004) 516 [hep-ex/0403022] [INSPIRE].

[37] BELLE-II collaboration, *B-flavor tagging at Belle II*, *Eur. Phys. J. C* **82** (2022) 283 [arXiv:2110.00790] [INSPIRE].

[38] BELLE collaboration, *A detailed test of the CsI(Tl) calorimeter for BELLE with photon beams of energy between 20-MeV and 5.4-GeV*, *Nucl. Instrum. Meth. A* **441** (2000) 401 [INSPIRE].

[39] BABAR collaboration, *Study of CP violation in Dalitz-plot analyses of $B^0 \to K^+K^-K^0_S, B^+ \to K^+K^-K^+$, and $B^+ \to K^0_S K^0_S K^+$*, *Phys. Rev. D* **85** (2012) 112010 [arXiv:1201.5897] [INSPIRE].

[40] E. Nakano, *Belle PID*, *Nucl. Instrum. Meth. A* **494** (2002) 402 [INSPIRE].

[41] CKMFITTER GROUP collaboration, *CP violation and the CKM matrix: Assessing the impact of the asymmetric B factories*, *Eur. Phys. J. C* **41** (2005) 1 [hep-ph/0406184] [INSPIRE].

[42] BABAR collaboration, *Measurement of CP observables in $B^{+-} \to D_{CP}K^{+-}$ decays and constraints on the CKM angle γ*, *Phys. Rev. D* **82** (2010) 072004 [arXiv:1007.0504] [INSPIRE].

[43] LHCb collaboration, *Measurement of CP observables in $B^\pm \to D^{(*)}K^\pm$ and $B^\pm \to D^{(*)}\pi^\pm$ decays using two-body D final states*, *JHEP* **04** (2021) 081 [arXiv:2012.09903] [INSPIRE].

JHEP05(2024)212

The Belle and Belle II collaboration

I. Adachi, L. Aggarwal, H. Aihara, N. Akopov, A. Aloisio, N. Anh Ky, D.M. Asner, H. Atmacan, T. Aushev, V. Aushev, M. Aversano, R. Ayad, V. Babu, H. Bae, S. Bahinipati, P. Bambade, Sw. Banerjee, M. Barrett, J. Baudot, M. Bauer, A. Baur, A. Beaubien, F. Becherer, J. Becker, P.K. Behera, K. Belous, J.V. Bennett, F.U. Bernlochner, V. Bertacchi, M. Bertemes, E. Bertholet, M. Bessner, S. Bettarini, B. Bhuyan, F. Bianchi, T. Bilka, D. Biswas, A. Bobrov, D. Bodrov, A. Bolz, A. Bondar, J. Borah, A. Bozek, M. Bračko, P. Branchini, R.A. Briere, T.E. Browder, A. Budano, S. Bussino, M. Campajola, L. Cao, G. Casarosa, C. Cecchi, J. Cerasoli, M.-C. Chang, P. Chang, P. Cheema, V. Chekelian, B.G. Cheon, K. Chilikin, K. Chirapatpimol, H.-E. Cho, K. Cho, S.-K. Choi, Y. Choi, S. Choudhury, J. Cochran, L. Corona, L.M. Cremaldi, T. Czank, S. Das, F. Dattola, E. De La Cruz-Burelo, S.A. De La Motte, G. de Marino, G. De Nardo, M. De Nuccio, G. De Pietro, R. de Sangro, M. Destefanis, S. Dey, A. De Yta-Hernandez, R. Dhamija, A. Di Canto, F. Di Capua, J. Dingfelder, Z. Doležal, I. Domínguez Jiménez, T.V. Dong, M. Dorigo, K. Dort, D. Dossett, S. Dreyer, S. Dubey, G. Dujany, P. Ecker, M. Eliachevitch, P. Feichtinger, T. Ferber, D. Ferlewicz, T. Fillinger, C. Finck, G. Finocchiaro, A. Fodor, F. Forti, A. Frey, B.G. Fulsom, A. Gabrielli, E. Ganiev, M. Garcia-Hernandez, R. Garg, A. Garmash, G. Gaudino, V. Gaur, A. Gaz, A. Gellrich, G. Ghevondyan, D. Ghosh, H. Ghumaryan, G. Giakoustidis, R. Giordano, A. Giri, B. Gobbo, R. Godang, O. Gogota, P. Goldenzweig, W. Gradl, S. Granderath, E. Graziani, D. Greenwald, Z. Gruberová, T. Gu, Y. Guan, K. Gudkova, S. Halder, Y. Han, T. Hara, K. Hayasaka, H. Hayashii, S. Hazra, C. Hearty, M.T. Hedges, A. Heidelbach, I. Heredia de la Cruz, M. Hernández Villanueva, A. Hershenhorn, T. Higuchi, E.C. Hill, M. Hoek, M. Hohmann, P. Horak, W.-S. Hou, C.-L. Hsu, T. Iijima, K. Inami, N. Ipsita, A. Ishikawa, S. Ito, R. Itoh, M. Iwasaki, P. Jackson, W.W. Jacobs, E.-J. Jang, Q.P. Ji, S. Jia, Y. Jin, A. Johnson, H. Junkerkalefeld, H. Kakuno, A.B. Kaliyar, J. Kandra, K.H. Kang, G. Karyan, T. Kawasaki, F. Keil, C. Ketter, C. Kiesling, C.-H. Kim, D.Y. Kim, K.-H. Kim, Y.-K. Kim, H. Kindo, K. Kinoshita, P. Kodyš, T. Koga, S. Kohani, K. Kojima, A. Korobov, S. Korpar, E. Kovalenko, R. Kowalewski, T.M.G. Kraetzschmar, P. Križan, P. Krokovny, T. Kuhr, M. Kumar, R. Kumar, K. Kumara, T. Kunigo, A. Kuzmin, Y.-J. Kwon, S. Lacaprara, Y.-T. Lai, T. Lam, L. Lanceri, J.S. Lange, M. Laurenza, R. Leboucher, F.R. Le Diberder, M.J. Lee, P. Leitl, D. Levit, P.M. Lewis, C. Li, J. Li, L.K. Li, Y. Li, J. Libby, Q.Y. Liu, Z.Q. Liu, D. Liventsev, S. Longo, T. Lueck, T. Luo, C. Lyu, Y. Ma, M. Maggiora, S.P. Maharana, R. Maiti, S. Maity, G. Mancinelli, R. Manfredi, E. Manoni, M. Mantovano, D. Marcantonio, S. Marcello, C. Marinas, L. Martel, C. Martellini, A. Martini, T. Martinov, L. Massaccesi, M. Masuda, T. Matsuda, D. Matvienko, S.K. Maurya, J.A. McKenna, R. Mehta, F. Meier, M. Merola, F. Metzner, M. Milesi, C. Miller, M. Mirra, K. Miyabayashi, R. Mizuk, G.B. Mohanty, N. Molina-Gonzalez, S. Mondal, S. Moneta, H.-G. Moser, M. Mrvar, R. Mussa, I. Nakamura, T. Nakano, Y. Nakazawa, A. Narimani Charan, M. Naruki, Z. Natkaniec, A. Natochii, L. Nayak, G. Nazaryan, N.K. Nisar, S. Nishida, S. Ogawa,

H. Ono, Y. Onuki, P. Oskin, F. Otani, P. Pakhlov, G. Pakhlova, A. Paladino, A. Panta, E. Paoloni, S. Pardi, K. Parham, H. Park, S.-H. Park, B. Paschen, A. Passeri, S. Patra, S. Paul, T.K. Pedlar, I. Peruzzi, R. Peschke, R. Pestotnik, F. Pham, M. Piccolo, L.E. Piilonen, P.L.M. Podesta-Lerma, T. Podobnik, S. Pokharel, C. Praz, S. Prell, E. Prencipe, M.T. Prim, H. Purwar, N. Rad, P. Rados, G. Raeuber, S. Raiz, M. Reif, S. Reiter, M. Remnev, I. Ripp-Baudot, G. Rizzo, L.B. Rizzuto, S.H. Robertson, M. Roehrken, J.M. Roney, A. Rostomyan, N. Rout, G. Russo, D. Sahoo, S. Sandilya, A. Sangal, L. Santelj, Y. Sato, V. Savinov, B. Scavino, C. Schmitt, G. Schnell, C. Schwanda, A.J. Schwartz, Y. Seino, A. Selce, K. Senyo, J. Serrano, M.E. Sevior, C. Sfienti, W. Shan, C. Sharma, X.D. Shi, T. Shillington, J.-G. Shiu, D. Shtol, A. Sibidanov, F. Simon, J.B. Singh, J. Skorupa, R.J. Sobie, M. Sobotzik, A. Soffer, A. Sokolov, E. Solovieva, S. Spataro, B. Spruck, M. Starič, P. Stavroulakis, S. Stefkova, Z.S. Stottler, R. Stroili, J. Strube, M. Sumihama, K. Sumisawa, W. Sutcliffe, H. Svidras, M. Takahashi, M. Takizawa, U. Tamponi, K. Tanida, F. Tenchini, A. Thaller, O. Tittel, R. Tiwary, D. Tonelli, E. Torassa, N. Toutounji, K. Trabelsi, I. Tsaklidis, M. Uchida, I. Ueda, S. Uehara, Y. Uematsu, T. Uglov, K. Unger, Y. Unno, K. Uno, S. Uno, P. Urquijo, Y. Ushiroda, S.E. Vahsen, R. van Tonder, G.S. Varner, K.E. Varvell, A. Vinokurova, V.S. Vismaya, L. Vitale, V. Vobbilisetti, R. Volpe, B. Wach, M. Wakai, S. Wallner, D. Wang, E. Wang, M.-Z. Wang, Z. Wang, A. Warburton, M. Watanabe, S. Watanuki, M. Welsch, C. Wessel, X.P. Xu, B.D. Yabsley, S. Yamada, W. Yan, S.B. Yang, J.H. Yin, K. Yoshihara, C.Z. Yuan, L. Zani, Y. Zhang, V. Zhilich, J.S. Zhou, Q.D. Zhou, V.I. Zhukova, R. Žlebčík

https://belle.kek.jp/
https://www.belle2.org/